Published in final edited form as:
Biochim Biophys Acta. 2015 January ; 1852(1): 61–69. doi:10.1016/j.bbadis.2014.10.010.

Triosephosphate Isomerase I170V Alters Catalytic Site, Enhances Stability and Induces Pathology in a *Drosophila* Model of TPI Deficiency

Bartholomew P. Roland[1,2], **Christopher G. Amrich**[3], **Charles J. Kammerer**[1,2], **Kimberly A. Stuchul**[1,2], **Samantha B. Larsen**[1,2], **Sascha Rode**[2,4], **Anoshé A. Aslam**[3], **Annie Heroux**[5], **Ronald Wetzel**[2,4], **Andrew P. VanDemark**[3,4], and **Michael J. Palladino**[1,2]

[1]Department of Pharmacology & Chemical Biology University of Pittsburgh School of Medicine, Pittsburgh, PA 15261

[2]Pittsburgh Institute for Neurodegenerative Diseases (PIND) University of Pittsburgh School of Medicine, Pittsburgh, PA 15261

[3]Department of Biological Sciences University of Pittsburgh, Pittsburgh, PA 15260

[4]Department of Structural Biology University of Pittsburgh School of Medicine, Pittsburgh, PA 15261

[5]Department of Biology, Brookhaven National Laboratory, Upton, NY 11973, USA

Abstract

Triosephosphate isomerase (TPI) is a glycolytic enzyme which homodimerizes for full catalytic activity. Mutations of the *TPI* gene elicit a disease known as TPI Deficiency, a glycolytic enzymopathy noted for its unique severity of neurological symptoms. Evidence suggests that TPI Deficiency pathogenesis may be due to conformational changes of the protein, likely affecting dimerization and protein stability. In this report, we genetically and physically characterize a human disease-associated TPI mutation caused by an I170V substitution. Human TPI^{I170V} elicits behavioral abnormalities in *Drosophila*. An examination of $hTPI^{I170V}$ enzyme kinetics revealed this substitution reduced catalytic turnover, while assessments of thermal stability demonstrated an

Corresponding author: Michael J. Palladino, Department of Pharmacology & Chemical Biology and the Pittsburgh Institute for Neurodegenerative Diseases (PIND), University of Pittsburgh School of Medicine, 3501 Fifth Ave., Pittsburgh, PA, USA, Tel: (412) 383-5900; Fax: (412) 648-7029; mjp44@pitt.edu.
Present address: Bartholomew P. Roland, Department of Biological Sciences, Vanderbilt University, Nashville, TN 37232, USA.

Author Contributions

BPR, CGA, KAS, SR, APV, and MJP designed the experiments; BPR, CGA, CJK, KAS, AAA, and SBL performed the research; BPR, CGA, SR, RW, AH, APV, and MJP analyzed the data; BPR, CGA, APV, and MJP wrote the manuscript.

Footnotes

Triosephosphate isomerase nomenclature has been divided between those studying the disease and those studying enzyme kinetics and structure. Authors discussing the pathology of TPI Deficiency typically use the abbreviation “TPI”. Conversely, early kinetic and structural studies of triosephosphate isomerase used the abbreviation “TIM”. This study is focused on determining the molecular mechanisms of a disease mutation, and for simplicity we have elected to use the abbreviation “TPI”.

increase in enzyme stability. The crystal structure of the homodimeric I170V mutant reveals changes in the geometry of critical residues within the catalytic pocket. Collectively these data reveal new observations of the structural and kinetic determinants of TPI deficiency pathology, providing new insights into disease pathogenesis.

Keywords

Triosephosphate isomerase; *Drosophila*; structure; Triosephosphate isomerase deficiency

1. Introduction

Functionally, TPI is a glycolytic enzyme that isomerizes dihydroxyacetone phosphate into glyceraldehyde 3-phosphate. This isomerization occurs at a non-linear step in the catabolic process, enhancing the efficiency of glycolysis, and is not required for the production of pyruvate. Mutations within the *TPI* coding region lead to a recessive disease known as TPI Deficiency, which is characterized by hemolytic anemia, neurologic dysfunction and often early death [1]. TPI Deficiency is unique among all other glycolytic enzymopathies in the presentation of severe neurologic deficits and the lack of ATP depletion [2]. It is not currently understood why mutations in a non-linear glycolytic enzyme elicit far greater pathology than other central glycolytic enzymes, though recent work has suggested that these neurologic differentiae are derived from a source other than general metabolic stress [3]. To date, only one of eleven physically distinct disease-associated TPI mutations has been structurally characterized [4, 5]. Additional physical analyses of disease-associated substitutions are clearly needed to understand the unique pathology associated with TPI Deficiency.

In the present report, we have investigated a poorly studied human disease-associated mutation of *TPI* that results in a valine substitution at position I170 of the protein, located within the catalytic lid of the enzyme. Previously, patients bearing the I170V substitution had only been identified in a *trans*-heterozygous state with the more common TPI^{E104D} missense allele [6]. These findings left it unclear whether I170V was viable as a homozygote, pathogenic, or simply lacked sufficient consanguinity for observation.

We have generated a *Drosophila* strain containing human TPI with an I170V mutation. *Drosophila* were selected for modeling this disease as it is currently the only model organism shown to recapitulate the complex neurologic dysfunction seen in human patients [7, 8]. These animals are homozygous viable, but *trans*-heterozygotes display behavioral abnormalities.

TPI utilizes the β/α triose isomerase (TIM) barrel to form its monomeric tertiary structure, but has only been described to function as a dimer *in vivo*. The TIM barrel motif is the structural base of over one hundred different enzymes, but was first identified in triosephosphate isomerase (TPI). TPI monomers *in vitro* exhibit little catalytic activity [9, 10], but attain catalytic perfection (diffusion-limited catalytic properties) upon dimerization [11]. Structural analyses of artificial monomeric TPI variants have revealed flexibility of normally rigid motifs in and around the catalytic pocket [9, 10]. These studies concluded

that dimerization facilitates the rigidification of the catalytic pocket through numerous Van der Waals forces, hydrogen bonds, and salt bridges between subunits within the dimer [12].

Two previous studies of a single disease-associated TPI substitution concluded that TPI deficiency was caused by reduced dimer stability [4, 13]. In contrast, however, our *in vitro* measurements of $hTPI^{I170V}$ thermal stability indicate an increase in enzyme stability. Further, the structure of $hTPI^{I170V}$ reveals a decoupling of the S96 residue from lid closure within the active site. We demonstrate that this alteration in catalytic site geometry leads to a decrease in catalytic turnover.

Our data establish that the disease-associated I170V substitution is sufficient to elicit pathology in an animal model, and alters both catalytic activity and thermal stability. These data reaffirm the importance of homodimer stability in TPI deficiency pathology. At the same time, the results suggest a counter-intuitive association of increased TPI stability and decreased TPI catalysis. These findings and their elucidation may be critical to understanding the unique pathology associated with TPI deficiency.

2.Methods

2.1 Mutagenesis and Genomic Engineering

The *pGE-hTPI*^{WT} construct was generated using human TPI (hTPI) coding region. The hTPI sequence was synthesized and recoded for *Drosophila* codon usage, while maintaining *Drosophila* intron-exon gene architecture and splicing, to ensure appropriate expression. The synthesized hTPI was designed to include flanking restriction sites for cloning into the *pGE-attBTPI*$^{+}$ plasmid [3]. Site directed mutagenesis was performed using the QuikChange Lightening Site-Directed Mutagenesis Kit (Agilent Technologies). Mutagenesis primers were generated (Integrated DNA Technologies) to introduce an Ile-to-Val codon change at position 170. Mutagenesis was performed with *pGE-hTPI*^{WT} and confirmed by sequencing. *TPI* GE was performed using previously published methods [3, 14, 15]. Briefly, the *PGX-TPI* founder animals were mated to *vasa-phiC31*$^{ZH\text{-}2A}$ animals expressing the integrase on the X chromosome and their progeny injected with *pGE-attBhTPI*^{WT}. Integration events were identified via the w^{+} phenotype and verified molecularly. The newly synthesized alleles were outcrossed to w^{1118} for five generations and mated to y^{1} w^{67c23} *P[y[+mDint2]=Crey]1b; D*/TM3,* Sb^{1} (Bloomington *Drosophila* Stock Center) to reduce the engineered locus. The *hTPI*^{I170V} allele was generated with similar methods.

2.2 Human TPI enzyme purification

Human TPI enzyme was purified as outlined previously [3]. Briefly, the coding sequence for *H. sapiens TPI* was cloned into the bacterial expression vector *pLC3* using standard techniques. The resulting plasmid directs expression of TPI containing N-terminal His_6- and MBP tags, both of which can be removed with TEV protease. TPI protein was expressed in BL21(DE3) Codon-Plus (RILP) *E. coli* (Agilent Technologies) grown in ZY auto-induction media (Studier, 2005) at room temperature for 24–30 hours. Cells were harvested by centrifugation, lysed via homogenization in 25 mM Tris pH 8.0, 500 mM NaCl, 10% glycerol, 5 mM imidazole, 1 mM β-mercaptoethanol and cleared by centrifugation at 30,000

× *g*. TPI was purified by nickel affinity chromatography followed by overnight TEV protease treatment to cleave the His_6-MBP tag from TPI. A second round of nickel affinity purification was performed to separate the His_6-MBP and TEV protease. TPI protein was further purified using anion-exchange chromatography (HiTrap-Q) followed by gel filtration (Sephacryl S-200, GE Healthcare). Peak fractions were concentrated to 4–8 mg/ml in 20 mM Tris pH 8.8, 25 mM NaCl, 2.0% glycerol and 1 mM β-mercaptoethanol using a Vivaspin concentrator (GE Healthcare). The purity was >99% as verified by SDS-PAGE.

2.3 TPI Enzyme Assays

Isomerase activity was determined using an NADH-linked assay as previously detailed [3, 16]. Initial velocity of the enzyme was calculated over a GAP (Sigma-Aldrich, St. Louis, MO, USA) range of 0.0094–4.23 mM; enzyme quantities as noted [Fig. 3]. All kinetic measurements were performed at 25°C to mimic *Drosophila* culture conditions, and measured in triplicate by monitoring the absorbance of NADH at 340 nm in a SpectraMax Plus 384 microplate reader (Molecular Devices). Initial velocities were taken during the linear phase of each reaction, and the data were fit to the Michaelis-Menten equation using nonlinear regression in Graphpad Prism 5.0b (GraphPad Software).

Lysate isomerase assays were performed as above. Lysates were generated as outlined previously [3] in 100 mM TEA pH 7.6 supplemented with cOmplete mini Protease Inhibitors (Roche Diagnostics). Lysates were diluted to 0.1 μg/μl in 100 mM TEA pH 7.6 + inhibitors and enzyme activity was assessed. Reactions were set up as above, using 0.752 mM GAP and 1 μg of lysate protein. Background NADH consumption was subtracted from each reaction by normalizing changes in absorbance to control reactions performed without GAP. All reactions were performed in triplicate.

2.4 Behavioral testing and lifespan analyses

Mechanical stress sensitivity was examined by vortexing the animals in a standard media vial for 20 seconds and measuring time to recovery, as previously [17, 18]. Thermal stress sensitivity was assessed by acutely shifting animals to 38°C and measuring time to paralysis, similar to the methods previously described [19, 20]. For this study, paralysis was defined as being ≥ 15 sec period of abnormal inactivity. All behavioral responses were capped at 600 seconds. Animal lifespans were performed at 25°C as previously described [19]. A two-tailed Student's t test was used to assess behavior, and lifespans were assessed with Log-rank (Mantel–Cox) survival tests.

2.5 Immunoblots

Animals were collected and aged 1–2 days at room temperature. Ten fly heads were obtained in triplicate from each genotype and processed as outlined previously [21]. Proteins were resolved by SDS–PAGE, transferred onto 0.45 μm PVDF membrane. The blots were blocked in 1% milk PBST, incubated with anti-TPI (1 : 5000; rabbit polyclonal FL-249; Santa Cruz Biotechnology) or anti-Beta tubulin (1 : 4,000; rabbit polyclonal d-140; Santa Cruz Biotechnology), and the appropriate HRP-conjugated secondary antibody. Blots were developed using enhanced chemiluminescence (Pierce). Densitometric analyses of the scanned films were performed digitally using ImageJ software (National Institutes of

Health) using sub-saturated exposures, and TPI signal was normalized to beta-tubulin. A two-tailed Student's t test was performed to assess differences TPI levels.

2.6 Circular dichroism and thermal stability

Circular dichroism (CD) thermal stability analyses were performed on a Jasco J-810 as outlined previously [4]. Briefly, samples were diluted to 350 μg/ml in 0.2 μm nylon-filtered 20 mM MOPS, 1 mM DTT, 1mM EDTA pH 7.4, and denaturation was monitored at 222 nm over 20–80°C at a rate of 0.267°C/min with a pitch of 0.2°C. Far-UV spectra were taken in 1× PBS at indicated temperatures for better resolution [4]. DL-glycerol-3-phosphate (Sigma), a TPI substrate analog [22–24], was added to a final concentration of 5 mM [25] and thermal stability reassessed. All spectral data were acquired 5 times per step, and performed in triplicate.

2.7 TPI crystallization and structure determination

Recombinant $hTPI^{WT}$ and $hTPI^{I170V}$ proteins were expressed and purified as described above. Initial TPI crystals were grown at 4°C using the sitting drop vapor diffusion method against a reservoir solution containing 34% PEG 2000 MME and 50 mM KBr. These initial crystals were improved by microseeding using a reservoir solution containing 30% PEG 2000 MME and 50 mM KBr. The crystals used for data collection grew to final dimensions of ~100 × 100 × 150 μm over the course of 3 days prior to harvesting. Crystals were cryoprotected by transition of the crystal into reservoir solution supplemented to 40% PEG 2000 MME and 20% glycerol followed by flash freezing in liquid nitrogen. Diffraction data were collected at the National Synchrotron Light Source on beamline X25 using a Pilatus 6M detector. Diffraction data were integrated, scaled, and merged using HKL2000 [26] using an $I/\sigma I$ cutoff of 2.0. $hTPI^{WT}$ crystals belong to the space group $P2_1$ (a = 47.92 Å, b = 48.85 Å, c = 93.97 Å; β = 103.66°) and contain a dimer in the asymmetric unit. Crystals of $hTPI^{I170V}$ belong to space group $P2_12_12_1$ (a = 64.92 Å, b = 73.64 Å, c = 91.77 Å), and also contain a dimer in the asymmetric unit. Initial phases for both $hTPI^{WT}$ and $hTPI^{I170V}$ were estimated via molecular replacement using a search model derived from an independent structure of human TPI (2JK2) [4]. The model was then refined and improved by manual rebuilding within Coot [27] combined with simulated annealing, positional, and anisotropic B factor refinement within Phenix. For $hTPI^{I170V}$, isotropic B-factor and TLS refinement was used. Model quality for both structures was assessed using MolProbity [28]. Structural figures were generated using PyMol (PyMOL Molecular Graphics System, Version 1.5.0.4, Schrödinger, LLC.). The coordinates and structure factors associated with hTPI and $hTPI^{I170V}$ structures have been deposited within the Protein Databank under accession codes 4POC and 4POD, respectively.

3. RESULTS

3.1 I170V induces behavioral dysfunction in *Drosophila*

Using our *Drosophila* genomic engineering (GE) system [3], we generated novel alleles of human TPI with an I170V substitution ($hTPI^{WT}$ and $hTPI^{I170V}$). GE is optimal for examining this type of dose-dependent loss-of-function disease, as it seamlessly places the modified alleles directly into the *Drosophila TPI* gene locus ensuring endogenous

expression at all developmental stages and in all tissues [14, 29]. The human *TPI* gene, which shares 63% identity with *Drosophila* TPI, was sufficient for *Drosophila* viability, confirming the strong conservation of TPI sequence, structure, and function.

Due to the relative abundance of null *TPI* alleles, many TPI deficient patients are genetically identified as *trans*-heterozygotes with a point mutation over a null allele [1, 2]. $hTPI^{I170V}$ proved to be homozygous viable, and preliminary experiments suggested the animals behaved similar to wild type. Therefore to more closely model a putative human condition, we generated *trans*-heterozygous populations and assessed two genotypes: $hTPI^{WT}/TPI^{null}$ and $hTPI^{I170V}/TPI^{null}$. The TPI^{null} allele is a deletion of two of the three exons of the TPI gene (formerly called TPI^{JS10}) [8].

We collected animals, aged them at 25°C, and examined their mechanical- and thermal-stress sensitivity and longevity, since these phenotypes have been shown to be hallmarks of *Drosophila* TPI Deficiency [3, 7, 8, 30]. Mechanical- and thermal-stress sensitivity were detected in $hTPI^{I170V}/TPI^{null}$ animals at both early (day 3 and 4) and late (day 20 and 22) time points, indicating progressive behavioral dysfunction [Fig. 1A,B]. A slight low-penetrant change in thermal stress sensitivity was noted in the heterozygous control population. These effects are not observed in homozygote WT animals, and we believe that this modest effect is likely a reflection of the heterozygote state ($hTPI^{WT}/TPI^{null}$). Interestingly, we did not detect a significant change in longevity when comparing $hTPI^{I170V}/TPI^{null}$ versus $hTPI^{WT}/TPI^{null}$ [Fig. 1C]. These results suggest *Drosophila* TPI Deficiency behavioral dysfunction and longevity phenotypes may be derived from different pathogenic sources.

3.2 *In vivo* TPI protein levels and enzyme activity

Having identified aberrant behavior in the $hTPI^{I170V}$ mutants, we sought to assess lysate isomerase activity and protein levels in this mutant. An analysis of wild type protein structure predicted that the I170V substitution would likely influence catalytic properties due to its positioning within the catalytic lid of the enzyme [Fig. 5]. Previous studies using a transgenic expression system in yeast identified a reduction in isomerase activity due to I170V [13], and our experiments measuring $hTPI^{WT}$ and $hTPI^{I170V}$ activity in animal lysates confirmed these observations [Fig. 2]. Of note though, a previous study performed by our lab failed to find a link between lysate isomerase activity, metabolic stress, and disease phenotypes [3]. This study suggested that a conformational change or depletion of cellular TPI elicited *Drosophila* TPI deficiency [3]. To examine the possibility that I170V may reduce protein levels in our system, we examined TPI levels in our newly generated alleles. Western blots indicated no changes in TPI protein levels due to the I170V substitution relative to TPI^{WT} [Fig. 2B,C]. Thus, the I170V mutation does not elicit pathology through a depletion of cellular TPI.

3.3 I170V reduces catalytic turnover and enhances enzyme stability *in vitro*

To examine how I170V may influence TPI catalysis, recombinant human $hTPI^{WT}$ and $hTPI^{I170V}$ was expressed and purified, and we examined their respective kinetic properties [Fig. 3C]. It should be noted that both enzymes displayed typical Michaelis-Menten

behavior [Fig. 3A,B]. hTPI^{WT} demonstrated properties similar to those previously published [31–34], while hTPI^{I170V} displayed a ~20 fold reduction in catalytic turnover and a ~30 fold reduction in K_m [Fig. 3C], a result in line with similar substitutions [34, 35]. The reduced hTPI^{I170V} turnover rate is likely the largest contributor to the altered Michaelis constant, though substrate affinity could also be an important contributor. Regardless, the reduced k_{cat} and K_m suggests the I170V substitution has shifted the enzyme toward a substrate-bound state.

Since previous studies had indicated that enzyme dimerization and stability were important molecular contributors to TPI deficiency [4, 13], we assessed the thermal stability of hTPI^{I170V} using circular dichroism (CD) [Fig. 4]. Over the past two decades several groups have characterized the folding and unfolding kinetics of TPI from numerous species [10, 36–42]. These studies have established that dimerization of TPI is a crucial determinant of protein stability, though several monomeric intermediates are also critical. Far-UV CD has been demonstrated to be capable of detecting the subtle changes in TPI unfolding. CD did not identify a marked change in protein folding at 20°C [Fig. 4B,C], but an assessment of thermal denaturing at 222 nm indicated a significant change in protein stability, with hTPI^{WT} and hTPI^{I170V} exhibiting monophasic denaturation with T_ms of 46.5°C and 59.4°C, respectively [Fig. 4A]. Previous studies have shown that CD measurements of TPI thermal denaturing elicit monophasic transitions [32, 43]. Importantly, these data indicate that hTPI^{I170V} enhances enzyme stability. Previously, Ralser and colleagues [13] noted that while E104D impaired WT:mut heterodimer associations in a yeast two-hybrid (Y2H) system, the I170V mutation appeared to increase these interactions. Our results suggest that this increase in Y2H signal was not likely due to aggregation or external factors, but that the I170V substitution may stabilize both homo-and heterodimer TPI species, yielding a more robust activation of the Y2H reporter.

The stability of the TPI dimer has previously been shown to be sensitive to substrate occupancy [38, 40]. Given the positioning of the I170V substitution near the catalytic pocket and the altered K_m, we examined whether hTPI^{I170V} stability would be as responsive to substrate administration as hTPI^{WT}. Using DL-glycerol-3-phosphate (DL-GP), a GAP substrate analog [22–24], we measured the stabilizing shift resulting from occupancy of the catalytic site. The addition of DL-GP to hTPI^{WT} resulted in a 3.7°C increase in stability (T_m 50.2°C), while DL-GP enhanced hTPI^{I170V} stability only 1.6°C (T_m 61.0°C) [Fig. 4A]. Denaturation of both hTPI^{I170V} and hTPI^{WT} was irreversible [Fig. 4B,C], in agreement with previous observations [4, 44, 45]. These results demonstrate that hTPI^{I170V} stability is less sensitive to substrate, and support a minor role for altered substrate affinity in the reduction of hTPI^{I170V} K_m.

3.4 hTPI^{I170V} decouples active site geometry from lid closure

To determine if we could elucidate the molecular mechanism responsible for altered hTPI^{I170V} catalytic properties, we determined structures for hTPI^{WT} and hTPI^{I170V} at 1.6 and 2.0 Å resolution, respectively, using x-ray crystallography (see Table 1). Fortunately, we were able to crystallize each protein in identical conditions, diminishing potential changes caused by differences in the buffering conditions. The overall fold of TPI is nearly

identical between $hTPI^{WT}$ and $hTPI^{I170V}$ (r.m.s.d. = 0.4 Å between 490 Cα atoms), consistent with our CD analyses. In both structures, a bromide ion from the crystallization conditions was found in the active site, as was a phosphate ion which co-purified with TPI [Fig. 5A,B]. The position of the phosphate moiety is conserved between our wild-type and I170V structures and closely matches phosphate groups from TPI co-crystallized with a variety of substrate and inhibitor molecules [Fig. 5B] [46–50], while the bromide ion [Fig. 5B, red] occupies the position taken by the triose moiety in structures of substrate bound TPI [46, 47, 50]. Previous mutagenesis and crystallography studies have described loop 6 as dynamic, and indeed NMR studies have shown breathing motions in this loop [51]. The lid is composed of three main components – N-hinge, a rigid tip, and Chinge [52]. The N-hinge residues 166–168 work in conjunction with the C-hinge (residues 174–176) to coordinate lid movements [44, 45, 53].

Residue I170 is located on the rigid tip of loop 6 of the TIM barrel fold of TPI. Loop 6 of TPI forms a “lid” over the catalytic pocket, and its closure over the substrate has been shown to prevent the dissociation of catalytic intermediates during substrate isomerization [54]. Within the context of loop 6, substrate binding has been demonstrated to result in the repositioning of residue I170 closer to the catalytic residue E165 [55]. The resulting orientation of the catalytic site is one in which the side chain of E165 is effectively clamped between residues I170 and L230, isolating the residue from bulk solvent and thereby enhancing its basicity [35, 56]. In the $hTPI^{I170V}$ structure presented here, both V170 and E165 are able to adopt conformations consistent with a closed pocket, indicating that the loss of the delta carbon in V170 does not prevent the protein from adopting the clamped configuration [Fig. 6A].

The side chains of S96 and E165 play critical roles in the catalytic mechanism for TPI. In an open lid conformation, S96 is positioned towards the catalytic pocket and hydrogen bonds with E165, stabilizing a non-catalytic conformation [Fig. 6B] [46, 57]. Upon substrate binding and lid closure, S96 rotates out of the catalytic pocket, breaking the hydrogen bond with the catalytic E165 which then shifts ~3 Å into the pocket, where it plays the role of a general base, abstracting a proton from the substrate as part of the catalytic reaction [58]. In our $hTPI^{I170V}$ structure, we find that the position of S96 side chain is rotated ~120° as compared to $hTPI^{WT}$, positioning its hydroxyl 1.9 Å toward the catalytic site despite having the lid in the closed position [Fig 6B]; note the similar orientation of S96 in closed-lid $hTPI^{I170V}$ and the superposed open-lid $hTPI^{WT}$ (2JK2) [Fig. 6C]. The position of H95 which serves as the general acid [47], and the catalytic E165 are found in the same positions as in substrate bound complexes indicating that these residues can still adopt positions consistent with catalysis [58]. Taken together, we conclude that the I170V substitution in human TPI appears to favor a closed lid orientation, and the I170V substitution decouples the orientation of S96 from lid closure.

4. DISCUSSION

Little is known about the pathogenesis of TPI deficiency. In the present report, we have pathologically and physically characterized a human disease-associated *TPI* mutation. We found that the I170V mutation was homozygous viable, yet when paired with a null allele

was capable of inducing behavioral dysfunction similar to a previously described pathogenic *Drosophila TPI* point mutation [7, 8]. These well-characterized fly behaviors are enriched for neurologic dysfunction, and therefore are believed to be analogs of the symptoms exhibited by human patients [59, 60].

Seeking a molecular explanation of $hTPI^{I170V}$ pathogenesis, the crystal structure of $hTPI^{I170V}$ revealed that the I170V substitution altered the molecular environment surrounding the active site. Specifically, the substitution of a smaller residue, valine, at the I170 position no longer makes the positions of S96 dependent on the conformation of the lid. Additionally, kinetic measurements revealed a significant reduction in enzyme turnover. These observations suggest three molecular sources of catalytic dysfunction.

First, the work of Knowles and colleagues has established that the catalytic rate of TPI is diffusion limited [11]. These kinetic studies have been recently complemented by solution NMR experiments, demonstrating the highly dynamic loop 6 is not gated by occupancy, but breathes irrespective of substrate, thereby facilitating its diffusion-limited catalytic properties [22, 61, 62]. In light of these results, it could be predicted that altering the rigid tip of loop 6 may change the rigid properties of the loop, though our crystal structure of $hTPI^{I170V}$ does not reveal any alterations in the relevant peptide backbone [Fig. 5,6]. Further, the hydrophobic nature of the loop is maintained, as well as its ability to facilitate the appropriate orientation of the catalytic E165 [Fig. 6A]. These data conclude that in the closed conformation, the gamma carbons of I170 and V170 are capable of producing the hydrophobic interactions necessary to align E165. Our observations are in line with observations made by Richard and colleagues, wherein a structurally equivalent I172V from *Trypanosoma brucei* produced a more moderate perturbation of TPI catalysis compared to that of I172A, which lacks the gamma carbon found in Ile and Val [35].

Secondly, the only other structure of a closed TPI complex with an inward S96 is one bound to a bulky competitive inhibitor (PDB: 1TSI) designed to promote contacts with residues in the periphery of the pocket [63]. In that structure, the rotation of S96 helped to form a novel hydrogen bond network with the inhibitor itself. We do not observe any interactions between S96 and the substrate-analogous bromide and phosphate ions in our I170V structure, but this does not preclude the possibility that S96 rotation directly inhibits substrate conversion. However, a substitution in this position has been shown to have a greater influence on the orientation of the catalytic H95 and E165, and exhibit no direct interactions between S96 and substrate [64].

Finally, a third possible source of reduced $hTPI^{I170V}$ turnover may derive from the decoupling of S96 within the context of loop 6 movement. As mentioned, the substitution of S96 has been demonstrated to influence TPI catalytic properties through alterations of H95 and E165 dynamics [64–66]. An S96P substitution was shown to mimic K_m and k_{cat} of I170V (chicken TPI^{S96P} (GAP), K_m (mM): 0.087, k_{cat} (s^{-1}): 64; $hTPI^{I170V}$, K_m: 0.049, k_{cat}: 75.8; wild type enzyme parameters were comparable) [64]. These kinetic deficiencies were linked to altered positioning of the catalytic base, E165. Further, the hydrogen bonding between S96 and the catalytic E165 may serve to assist the torsion of the proceeding N hinge (P166-V167-W168) of loop 6. Several research groups have posited the rotation of the

N hinge to be the physical mechanism responsible for loop 6 movement, with hinge mutations also resulting in reduced enzyme turnover [45, 53]. Uncoupling S96 movement from lid closure in hTPI^{I170V} would stabilize the closed lid conformation in the substrate-bound and –unbound states, as well as potentially reduce E165 mobility, with either of these two possibilities influencing enzyme turnover. Although our crystallography data do not unequivocally establish that impaired S96-E165 hydrogen bonding is the primary affector of hTPI^{I170V} catalysis, the data suggest this to be the simplest explanation for our observed kinetics.

The only previously crystallized human disease-associated TPI substitution, E104D, indicated a miscoordination of a conserved water network at the homodimer interface. This alteration of the dimer interface elicited a reduction in hTPI^{E104D} stability, but did not change catalytic activity [4]. Our data establish the I170V substitution alters catalytic properties while enhancing TPI stability relative to hTPI^{WT} [Fig. 4,5]. As such, hTPI^{I170V} is the first example of a disease associated TPI mutation that enhances enzyme stability.

Although an unanticipated and exciting result, the structure of hTPI^{I170V} does not yield any insight into why we observe dramatic changes in thermal stability. Indeed, no marked changes are observed between hTPI^{WT} and hTPI^{I170V} at any location other than the catalytic site [Fig. 5]. Therefore, these structural data lead us to speculate that lid orientation is likely responsible for the changes in enzyme stability. Preferential lid closure would provide additional protection from bulk solvent, and increase overall solvent entropy; a result borne out by the substrate-induced stabilization of hTPI^{WT}. Interestingly, the preferentially closed lid of hTPI^{I170V}, even in the absence of substrate, could be predicted to reduce the mutant enzyme's sensitivity to substrate-induced TPI stabilization, in agreement with our data [Fig. 4A].

The effect of the I170V substitution *in vivo* appears to be complex. The observed reduction in lysate *hTPI^{I170V}* catalytic activity underlined the altered active-site geometry, a result corroborated by a previous study in yeast lysates [13]. Our measurements of catalytic turnover and K_m demonstrated that the I170V substitution reduces both parameters. It is important to note that measurements of GAP concentrations in human tissue suggest that the hTPI^{I170V} enzyme operates in the cell under conditions much closer to saturation compared to the hTPI^{WT} enzyme. The normal concentration range of GAP in humans has been reported to be in the 1–20 μM range [67, 68], while our K_m values for GAP are 1.4±0.1 mM for hTPI^{WT} and 0.049±0.014 mM for hTPI^{I170V}. These data indicate that each enzyme is likely efficient enough to meet resting demands. However, recent work established that downstream glycolytic intermediates can competitively inhibit TPI [34]. Given that these competitive inhibitors will selectively increase the apparent K_m, a tissue environment of increased glycolytic flux would render hTPI^{I170V}'s efficiency limited to its catalytic turnover. We did not observe abnormal behaviors without stress induction, or changes in longevity, supporting the capacity of hTPI^{I170V} to meet resting needs. However, behavioral abnormalities were noted upon stress induction, suggesting the exacerbation of an acute affect.

Irrespective of the molecular mechanism, the findings that hTPI^{I170V} induces pathology and is characterized by decreased catalysis and increased stability demonstrates that reduced TPI stability alone is not the only means to achieve pathology. Considering these observations and those of others in the field, we propose that localized, not bulk TPI activity, is necessary for normal behavior.

The proposal that localized activity could be a critical determinant of pathology stems from the preeminent finding that hTPI^{I170V} has a dramatic effect on enzyme kinetic parameters. Previous work has demonstrated that a catalytically inactive TPI allele can complement the toxic TPI^{M80T} substitution. This study concluded that TPI Deficiency is not correlated with lysate isomerase activity or metabolic stress [3], yet did not exclude the role of TPI in cellular redox levels [69], or the possibility of small environments of localized catalytic activity. These micro-environments may be tissues or subcellular locations with unusually high concentrations of DHAP, GAP, or glycolytic intermediates acting as inhibitors. One such location with high glycolytic flux is the neuronal synapse. The synapse is a subcellular locale that depends largely on glycolytic ATP [70]. Further, glycolysis is not only spatially but temporally regulated in this tissue, with activity promoting acute increases in glycolytic flux [70]. In this way, a spatial or temporal increase in TPI substrate at the synapse may lead to localized deficiencies caused by the low catalytic turnover of hTPI^{I170V}. However, other tissues could be just as important, and it is unclear whether glycolysis is the central pathway determining pathology.

TPI activity contributes to the glycerol synthesis pathway, glycolysis, the pentose-phosphate pathway, and the glycerol 3-phosphate NADH shuttle. Few, if any mutations in the aforementioned pathways have been linked to patient neurological dysfunction, and none with the severity of TPI Deficiency. These observations fail to suggest a singular biochemical pathway that could be responsible for TPI Deficiency. Additional work will be needed to explore the putative importance of localized catalytic environments, the participating biochemical pathways, and their contribution to the unique pathology associated with TPI deficiency.

In conclusion, the data presented in this study demonstrate the pathogenic nature of a previously understudied human mutation, and illustrate its unique kinetic and stability properties with a crystal structure. Using this structure, we suggest a molecular mechanism responsible the pathogenic properties of hTPI^{I170V}. These results are critical for directing future experimentation surrounding the largely understudied role of TPI in animal physiology, the pathogenesis of TPI Deficiency, and future therapeutic strategies.

Acknowledgements

The authors would like to thank Atif Towheed, Kenneth Drombosky, and Aaron Talsma for their helpful discussions. This work was supported by a fellowship from Achievement Rewards for College Scientists: Pittsburgh Chapter [BPR]; and the National Institutes of Health [grant numbers R01 GM103369 MJP and APV, R01 GM097204 APV, and T32 GM8424-17 BPR].

Abbreviations

TPI	triosephosphate isomerase
TIM	triose isomerase
GAP	glyceraldehyde 3-phosphate
DHAP	dihydroxyacetone phosphate
CD	circular dichroism
GE	genomic engineering
DL-GP	DL-glycerol-3-phosphate.

REFERENCES

1. Schneider AS. Triosephosphate isomerase deficiency: historical perspectives and molecular aspects. Baillieres Best Pract Res Clin Haematol. 2000; 13:119–140. [PubMed: 10916682]
2. Orosz F, Olah J, Ovadi J. Triosephosphate isomerase deficiency: facts and doubts. IUBMB Life. 2006; 58:703–715. [PubMed: 17424909]
3. Roland BP, Stuchul KA, Larsen SB, Amrich CG, Vandemark AP, Celotto AM, Palladino MJ. Evidence of a triosephosphate isomerase non-catalytic function crucial to behavior and longevity. J Cell Sci. 2013; 126:3151–3158. [PubMed: 23641070]
4. Rodriguez-Almazan C, Arreola R, Rodriguez-Larrea D, Aguirre-Lopez B, de Gomez-Puyou MT, Perez-Montfort R, Costas M, Gomez-Puyou A, Torres-Larios A. Structural basis of human triosephosphate isomerase deficiency: mutation E104D is related to alterations of a conserved water network at the dimer interface. J Biol Chem. 2008; 283:23254–23263. [PubMed: 18562316]
5. Orosz F, Olah J, Ovadi J. Triosephosphate isomerase deficiency: new insights into an enigmatic disease. Biochim Biophys Acta. 2009; 1792:1168–1174. [PubMed: 19786097]
6. Arya R, Lalloz MR, Bellingham AJ, Layton DM. Evidence for founder effect of the Glu104Asp substitution and identification of new mutations in triosephosphate isomerase deficiency. Hum Mutat. 1997; 10:290–294. [PubMed: 9338582]
7. Gnerer JP, Kreber RA, Ganetzky B. wasted away, a Drosophila mutation in triosephosphate isomerase, causes paralysis, neurodegeneration, and early death. Proc Natl Acad Sci U S A. 2006; 103:14987–14993. [PubMed: 17008404]
8. Celotto AM, Frank AC, Seigle JL, Palladino MJ. Drosophila model of human inherited triosephosphate isomerase deficiency glycolytic enzymopathy. Genetics. 2006; 174:1237–1246. [PubMed: 16980388]
9. Schliebs W, Thanki N, Eritja R, Wierenga R. Active site properties of monomeric triosephosphate isomerase (monoTIM) as deduced from mutational and structural studies. Protein Sci. 1996; 5:229–239. [PubMed: 8745400]
10. Schliebs W, Thanki N, Jaenicke R, Wierenga RK. A double mutation at the tip of the dimer interface loop of triosephosphate isomerase generates active monomers with reduced stability. Biochemistry. 1997; 36:9655–9662. [PubMed: 9245397]
11. Blacklow SC, Raines RT, Lim WA, Zamore PD, Knowles JR. Triosephosphate isomerase catalysis is diffusion controlled. Appendix: Analysis of triose phosphate equilibria in aqueous solution by 31P NMR. Biochemistry. 1988; 27:1158–1167. [PubMed: 3365378]
12. Norledge BV, Lambeir AM, Abagyan RA, Rottmann A, Fernandez AM, Filimonov VV, Peter MG, Wierenga RK. Modeling, mutagenesis, and structural studies on the fully conserved phosphate-binding loop (loop 8) of triosephosphate isomerase: toward a new substrate specificity. Proteins. 2001; 42:383–389. [PubMed: 11151009]
13. Ralser M, Heeren G, Breitenbach M, Lehrach H, Krobitsch S. Triose phosphate isomerase deficiency is caused by altered dimerization--not catalytic inactivity--of the mutant enzymes. PLoS One. 2006; 1:e30. [PubMed: 17183658]

14. Huang J, Zhou W, Dong W, Watson AM, Hong Y. From the Cover: Directed, efficient, and versatile modifications of the Drosophila genome by genomic engineering. Proc Natl Acad Sci U S A. 2009; 106:8284–8289. [PubMed: 19429710]
15. Huang J, Zhou W, Watson AM, Jan YN, Hong Y. Efficient ends-out gene targeting in Drosophila. Genetics. 2008; 180:703–707. [PubMed: 18757917]
16. Williams JC, Zeelen JP, Neubauer G, Vriend G, Backmann J, Michels PA, Lambeir AM, Wierenga RK. Structural and mutagenesis studies of leishmania triosephosphate isomerase: a point mutation can convert a mesophilic enzyme into a superstable enzyme without losing catalytic power. Protein Eng. 1999; 12:243–250. [PubMed: 10235625]
17. Ganetzky B, Loughney K, Wu CF. Analysis of mutations affecting sodium channels in Drosophila. Ann N Y Acad Sci. 1986; 479:325–337. [PubMed: 2433999]
18. Ganetzky B, Wu CF. Indirect Suppression Involving Behavioral Mutants with Altered Nerve Excitability in DROSOPHILA MELANOGASTER. Genetics. 1982; 100:597–614. [PubMed: 17246073]
19. Palladino MJ, Bower JE, Kreber R, Ganetzky B. Neural dysfunction and neurodegeneration in Drosophila Na+/K+ ATPase alpha subunit mutants. J Neurosci. 2003; 23:1276–1286. [PubMed: 12598616]
20. Palladino MJ, Hadley TJ, Ganetzky B. Temperature-sensitive paralytic mutants are enriched for those causing neurodegeneration in Drosophila. Genetics. 2002; 161:1197–1208. [PubMed: 12136022]
21. Hrizo SL, Palladino MJ. Hsp70- and Hsp90-mediated proteasomal degradation underlies TPI sugarkill pathogenesis in Drosophila. Neurobiol Dis. 2010; 40:676–683. [PubMed: 20727972]
22. Rozovsky S, McDermott AE. The time scale of the catalytic loop motion in triosephosphate isomerase. J Mol Biol. 2001; 310:259–270. [PubMed: 11419951]
23. Fenn RH, Marshall GE. The stereochemical structure of disodium DL-glycerol 3-phosphate hexahydrate, the D isomer of which is an inhibitor of triose phosphate isomerase. Biochem J. 1972; 130:1–10. [PubMed: 4655425]
24. Nickbarg EB, Knowles JR. Triosephosphate isomerase: energetics of the reaction catalyzed by the yeast enzyme expressed in Escherichia coli. Biochemistry. 1988; 27:5939–5947. [PubMed: 3056516]
25. Johnson LN, Wolfenden R. Changes in absorption spectrum and crystal structure of triose phosphate isomerase brought about by 2-phosphoglycollate, a potential transition state analogue. J Mol Biol. 1970; 47:93–100. [PubMed: 5461000]
26. Otwinowski Z, Minor W. Processing of X-ray diffraction data collected in oscillation mode. Method Enzymol. 1997; 276:307–326.
27. Emsley P, Lohkamp B, Scott WG, Cowtan K. Features and development of Coot. Acta Crystallogr D Biol Crystallogr. 2010; 66:486–501. [PubMed: 20383002]
28. Davis IW, Leaver-Fay A, Chen VB, Block JN, Kapral GJ, Wang X, Murray LW, Arendall WB 3rd, Snoeyink J, Richardson JS, Richardson DC. MolProbity: all-atom contacts and structure validation for proteins and nucleic acids. Nucleic Acids Res. 2007; 35:W375–W383. [PubMed: 17452350]
29. Huang J, Huang L, Chen YJ, Austin E, Devor CE, Roegiers F, Hong Y. Differential regulation of adherens junction dynamics during apical-basal polarization. J Cell Sci. 2007; 124:4001–4013. [PubMed: 22159415]
30. Seigle JL, Celotto AM, Palladino MJ. Degradation of functional triose phosphate isomerase protein underlies sugarkill pathology. Genetics. 2008; 179:855–862. [PubMed: 18458110]
31. Mainfroid V, Terpstra P, Beauregard M, Frere JM, Mande SC, Hol WG, Martial JA, Goraj K. Three hTIM mutants that provide new insights on why TIM is a dimer. J Mol Biol. 1996; 257:441–456. [PubMed: 8609635]
32. Peimbert M, Dominguez-Ramirez L, Fernandez-Velasco DA. Hydrophobic repacking of the dimer interface of triosephosphate isomerase by in silico design and directed evolution. Biochemistry. 2008; 47:5556–5564. [PubMed: 18439027]
33. Hernandez-Alcantara G, Torres-Larios A, Enriquez-Flores S, Garcia-Torres I, Castillo-Villanueva A, Mendez ST, de la Mora-de la Mora I, Gomez-Manzo S, Torres-Arroyo A, Lopez-Velazquez G,

Reyes-Vivas H, Oria-Hernandez J. Structural and functional perturbation of giardia lamblia triosephosphate isomerase by modification of a non-catalytic, non-conserved region. PLoS One. 2013; 8:e69031. [PubMed: 23894402]

34. Gruning NM, Du D, Keller MA, Luisi BF, Ralser M. Inhibition of triosephosphate isomerase by phosphoenolpyruvate in the feedback-regulation of glycolysis. Open Biol. 2014; 4:130232. [PubMed: 24598263]
35. Malabanan MM, Koudelka AP, Amyes TL, Richard JP. Mechanism for activation of triosephosphate isomerase by phosphite dianion: the role of a hydrophobic clamp. J Am Chem Soc. 2012; 134:10286–10298. [PubMed: 22583393]
36. Chanez-Cardenas ME, Fernandez-Velasco DA, Vazquez-Contreras E, Coria R, Saab-Rincon G, Perez-Montfort R. Unfolding of triosephosphate isomerase from Trypanosoma brucei: identification of intermediates and insight into the denaturation pathway using tryptophan mutants. Arch Biochem Biophys. 2002; 399:117–129. [PubMed: 11888197]
37. Chanez-Cardenas ME, Perez-Hernandez G, Sanchez-Rebollar BG, Costas M, Vazquez-Contreras E. Reversible equilibrium unfolding of triosephosphate isomerase from Trypanosoma cruzi in guanidinium hydrochloride involves stable dimeric and monomeric intermediates. Biochemistry. 2005; 44:10883–10892. [PubMed: 16086591]
38. Gonzalez-Mondragon E, Zubillaga RA, Hernandez-Arana A. Effect of a specific inhibitor on the unfolding and refolding kinetics of dimeric triosephosphate isomerase: establishing the dimeric and similarly structured nature of the main transition states on the forward and backward reactions. Biophys Chem. 2007; 125:172–178. [PubMed: 16919384]
39. Mixcoha-Hernandez E, Moreno-Vargas LM, Rojo-Dominguez A, Benitez-Cardoza CG. Thermal-unfolding reaction of triosephosphate isomerase from Trypanosoma cruzi. Protein J. 2007; 26:491–498. [PubMed: 17763928]
40. Tellez LA, Blancas-Mejia LM, Carrillo-Nava E, Mendoza-Hernandez G, Cisneros DA, Fernandez-Velasco DA. Thermal unfolding of triosephosphate isomerase from Entamoeba histolytica: dimer dissociation leads to extensive unfolding. Biochemistry. 2008; 47:11665–11673. [PubMed: 18837510]
41. Lambeir AM, Backmann J, Ruiz-Sanz J, Filimonov V, Nielsen JE, Kursula I, Norledge BV, Wierenga RK. The ionization of a buried glutamic acid is thermodynamically linked to the stability of Leishmania mexicana triose phosphate isomerase. Eur J Biochem. 2000; 267:2516–2524. [PubMed: 10785370]
42. Thanki N, Zeelen JP, Mathieu M, Jaenicke R, Abagyan RA, Wierenga RK, Schliebs W. Protein engineering with monomeric triosephosphate isomerase (monoTIM): the modelling and structure verification of a seven-residue loop. Protein Eng. 1997; 10:159–167. [PubMed: 9089815]
43. Benitez-Cardoza CG, Rojo-Dominguez A, Hernandez-Arana A. Temperature-induced denaturation and renaturation of triosephosphate isomerase from Saccharomyces cerevisiae: evidence of dimerization coupled to refolding of the thermally unfolded protein. Biochemistry. 2001; 40:9049–9058. [PubMed: 11467968]
44. Sun J, Sampson NS. Determination of the amino acid requirements for a protein hinge in triosephosphate isomerase. Protein Sci. 1998; 7:1495–1505. [PubMed: 9684881]
45. Xiang J, Sun J, Sampson NS. The importance of hinge sequence for loop function and catalytic activity in the reaction catalyzed by triosephosphate isomerase. J Mol Biol. 2001; 307:1103–1112. [PubMed: 11286559]
46. Zhang Z, Sugio S, Komives EA, Liu KD, Knowles JR, Petsko GA, Ringe D. Crystal structure of recombinant chicken triosephosphate isomerase-phosphoglycolohydroxamate complex at 1.8-A resolution. Biochemistry. 1994; 33:2830–2837. [PubMed: 8130195]
47. Jogl G, Rozovsky S, McDermott AE, Tong L. Optimal alignment for enzymatic proton transfer: structure of the Michaelis complex of triosephosphate isomerase at 1.2-A resolution. Proc Natl Acad Sci U S A. 2003; 100:50–55. [PubMed: 12509510]
48. Mande SC, Mainfroid V, Kalk KH, Goraj K, Martial JA, Hol WG. Crystal structure of recombinant human triosephosphate isomerase at 2.8 A resolution. Triosephosphate isomerase-related human genetic disorders and comparison with the trypanosomal enzyme. Protein Sci. 1994; 3:810–821. [PubMed: 8061610]

49. Noble ME, Wierenga RK, Lambeir AM, Opperdoes FR, Thunnissen AM, Kalk KH, Groendijk H, Hol WG. The adaptability of the active site of trypanosomal triosephosphate isomerase as observed in the crystal structures of three different complexes. Proteins. 1991; 10:50–69. [PubMed: 2062828]
50. Gayathri P, Banerjee M, Vijayalakshmi A, Balaram H, Balaram P, Murthy MR. Biochemical and structural characterization of residue 96 mutants of Plasmodium falciparum triosephosphate isomerase: active-site loop conformation, hydration and identification of a dimer-interface ligand-binding site. Acta Crystallogr D Biol Crystallogr. 2009; 65:847–857. [PubMed: 19622869]
51. Massi F, Wang C, Palmer AG 3rd. Solution NMR and computer simulation studies of active site loop motion in triosephosphate isomerase. Biochemistry. 2006; 45:10787–10794. [PubMed: 16953564]
52. Kursula I, Salin M, Sun J, Norledge BV, Haapalainen AM, Sampson NS, Wierenga RK. Understanding protein lids: structural analysis of active hinge mutants in triosephosphate isomerase. Protein Eng Des Sel. 2004; 17:375–382. [PubMed: 15166315]
53. Sun J, Sampson NS. Understanding protein lids: kinetic analysis of active hinge mutants in triosephosphate isomerase. Biochemistry. 1999; 38:11474–11481. [PubMed: 10471299]
54. Pompliano DL, Peyman A, Knowles JR. Stabilization of a reaction intermediate as a catalytic device: definition of the functional role of the flexible loop in triosephosphate isomerase. Biochemistry. 1990; 29:3186–3194. [PubMed: 2185832]
55. Kursula I, Wierenga RK. Crystal structure of triosephosphate isomerase complexed with 2-phosphoglycolate at 0.83-A resolution. J Biol Chem. 2003; 278:9544–9551. [PubMed: 12522213]
56. Malabanan MM, Nitsch-Velasquez L, Amyes TL, Richard JP. Magnitude and origin of the enhanced basicity of the catalytic glutamate of triosephosphate isomerase. J Am Chem Soc. 2013; 135:5978–5981. [PubMed: 23560625]
57. Lolis E, Alber T, Davenport RC, Rose D, Hartman FC, Petsko GA. Structure of yeast triosephosphate isomerase at 1.9-A resolution. Biochemistry. 1990; 29:6609–6618. [PubMed: 2204417]
58. Harris TK, Abeygunawardana C, Mildvan AS. NMR studies of the role of hydrogen bonding in the mechanism of triosephosphate isomerase. Biochemistry. 1997; 36:14661–14675. [PubMed: 9398185]
59. Parker L, Howlett IC, Rusan ZM, Tanouye MA. Seizure and epilepsy: studies of seizure disorders in Drosophila. Int Rev Neurobiol. 2011; 99:1–21. [PubMed: 21906534]
60. Song J, Tanouye MA. From bench to drug: human seizure modeling using Drosophila. Prog Neurobiol. 2008; 84:182–191. [PubMed: 18063465]
61. Rozovsky S, Jogl G, Tong L, McDermott AE. Solution-state NMR investigations of triosephosphate isomerase active site loop motion: ligand release in relation to active site loop dynamics. J Mol Biol. 2001; 310:271–280. [PubMed: 11419952]
62. Williams JC, McDermott AE. Dynamics of the flexible loop of triosephosphate isomerase: the loop motion is not ligand gated. Biochemistry. 1995; 34:8309–8319. [PubMed: 7599123]
63. Verlinde CL, Witmans CJ, Pijning T, Kalk KH, Hol WG, Callens M, Opperdoes FR. Structure of the complex between trypanosomal triosephosphate isomerase and N-hydroxy-4-phosphono-butanamide: binding at the active site despite an "open" flexible loop conformation. Protein Sci. 1992; 1:1578–1584. [PubMed: 1304889]
64. Zhang Z, Komives EA, Sugio S, Blacklow SC, Narayana N, Xuong NH, Stock AM, Petsko GA, Ringe D. The role of water in the catalytic efficiency of triosephosphate isomerase. Biochemistry. 1999; 38:4389–4397. [PubMed: 10194358]
65. Komives EA, Lougheed JC, Liu K, Sugio S, Zhang Z, Petsko GA, Ringe D. The structural basis for pseudoreversion of the E165D lesion by the secondary S96P mutation in triosephosphate isomerase depends on the positions of active site water molecules. Biochemistry. 1995; 34:13612–13621. [PubMed: 7577950]
66. Komives EA, Lougheed JC, Zhang Z, Sugio S, Narayana N, Xuong NH, Petsko GA, Ringe D. The structural basis for pseudoreversion of the H95N lesion by the secondary S96P mutation in triosephosphate isomerase. Biochemistry. 1996; 35:15474–15484. [PubMed: 8952501]

67. Olah J, Orosz F, Puskas LG, Hackler L Jr, Horanyi M, Polgar L, Hollan S, Ovadi J. Triosephosphate isomerase deficiency: consequences of an inherited mutation at mRNA, protein and metabolic levels. Biochem J. 2005; 392:675–683. [PubMed: 16086671]

68. Gilroy TE, Brewer GJ, Sing CF. Genetic control of glycolysis in human erythrocytes. Genetics. 1980; 94:719–732. [PubMed: 7399259]

69. Hrizo SL, Fisher IJ, Long DR, Hutton JA, Liu Z, Palladino MJ. Early mitochondrial dysfunction leads to altered redox chemistry underlying pathogenesis of TPI deficiency. Neurobiol Dis. 2013; 54:289–296. [PubMed: 23318931]

70. Rangaraju V, Calloway N, Ryan TA. Activity-driven local ATP synthesis is required for synaptic function. Cell. 2014; 156:825–835. [PubMed: 24529383]

Highlights

- The human *TPI*^{I170V} missense allele is pathogenic.
- Substituting I170V alters catalytic site geometry.
- hTPI^{I170V} reduces catalytic turnover and enhances stability.

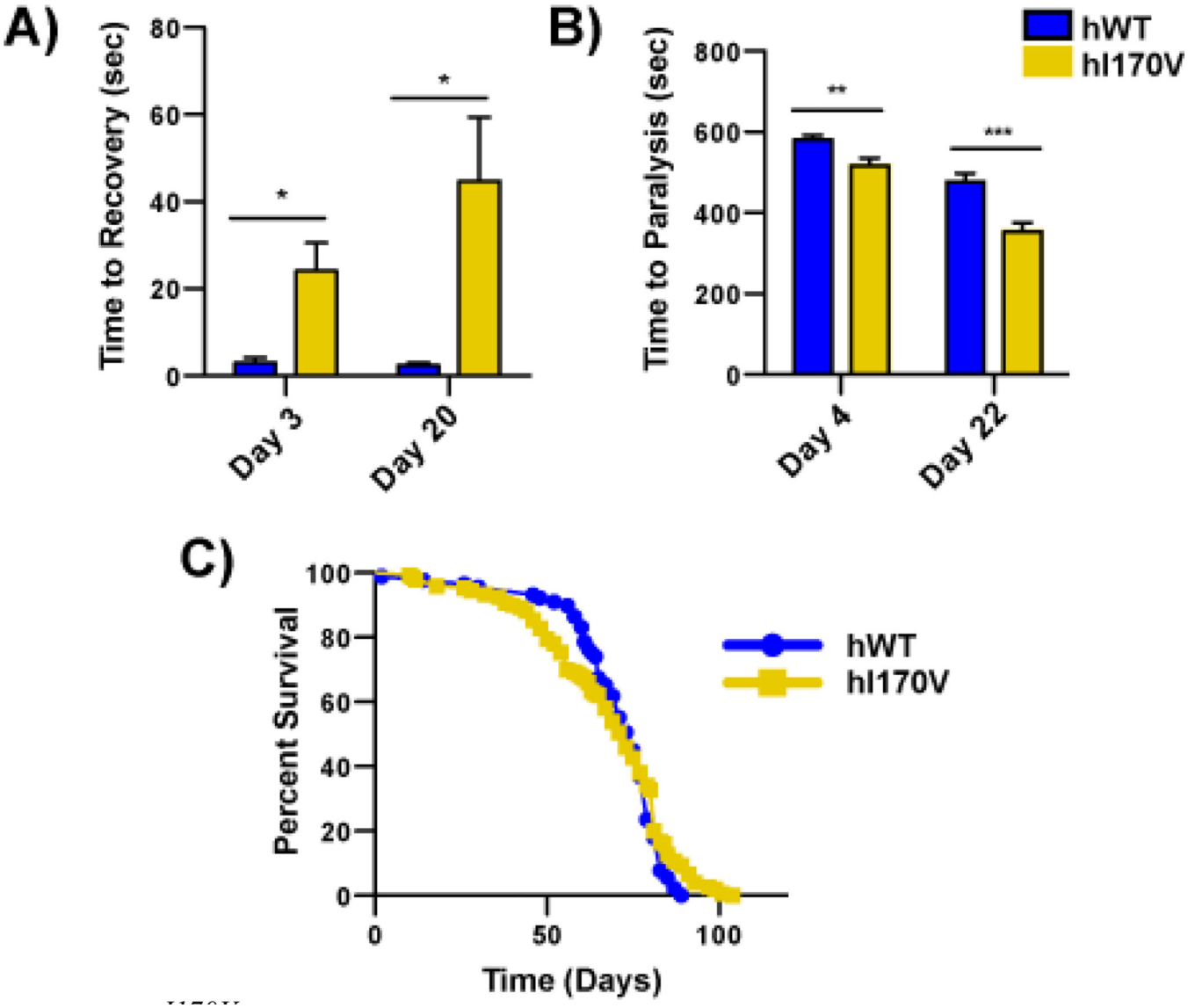

Fig. 1.

hTPI^{I170V} is characterized by behavioral dysfunction but not reduced longevity. *hTPI*^{I170V}/*TPI*^{null} exhibits mechanical (A) and thermal (B) stress sensitivity relative to *hTPI*^{WT}/*TPI*^{null}, n≥20. Conversely, *hTPI*^{I170V}/*TPI*^{null} demonstrated similar lifespans (C) as *hTPI*^{WT}/*TPI*^{null}, n≥89. * indicates p<0.05, ** p<0.01, and *** p<0.001. Error bars indicate S.E.M.

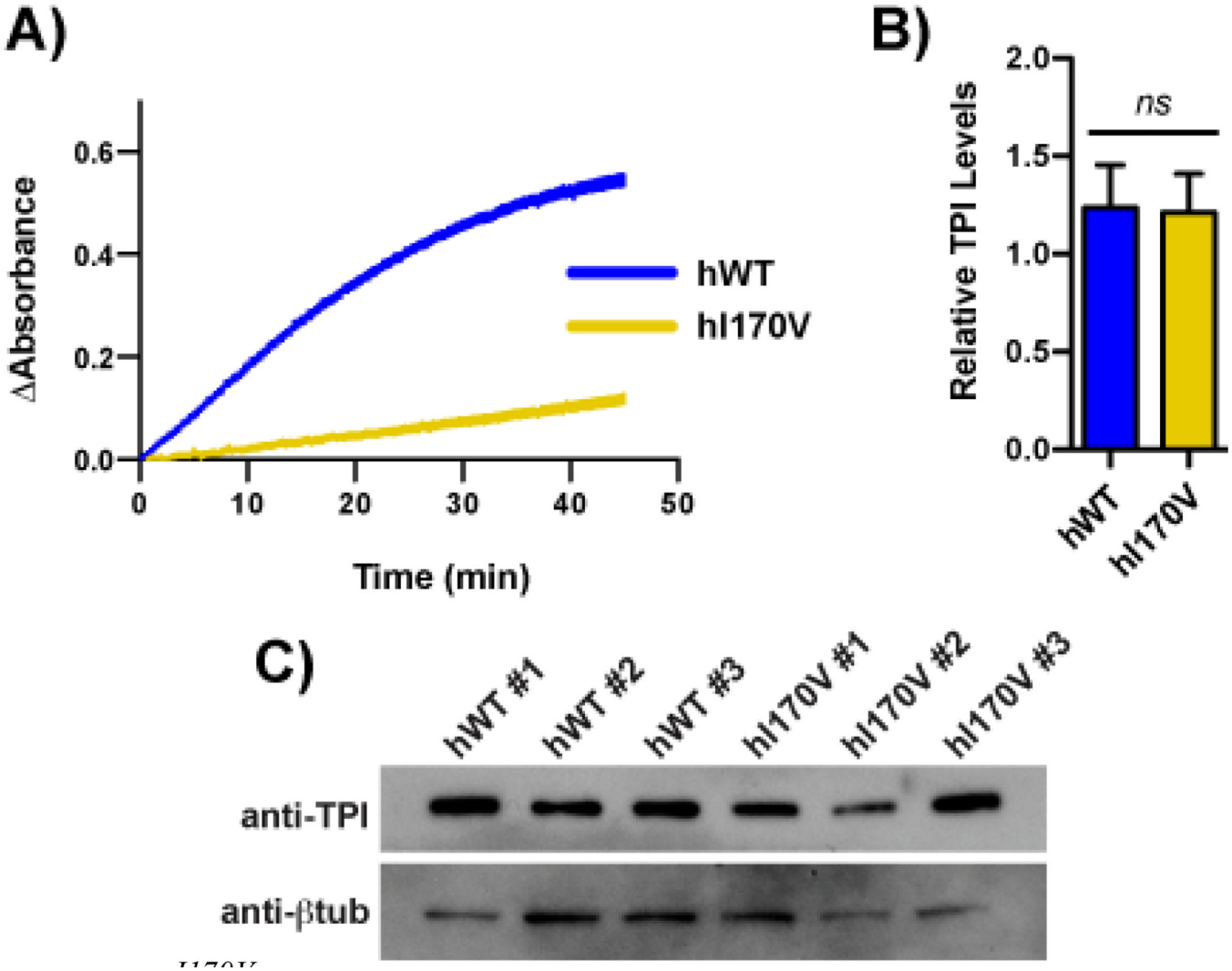

Fig. 2.

hTPI^{I170V} exhibits reduced catalysis and normal cellular TPI levels. Isomerase assays reveal *hTPI*^{I170V}*/TPI*^{null} reduces lysate TPI activity relative to *hTPI*^{WT}*/TPI*^{null} (A), n=3. Independent samples of *hTPI*^{WT}*/TPI*^{null} and *hTPI*^{I170V}*/TPI*^{null} (#1,#2,#3) demonstrate similar levels of cellular TPI (C), with quantification (B), n=3. *ns* indicates no significance. Error bars represent S.E.M.

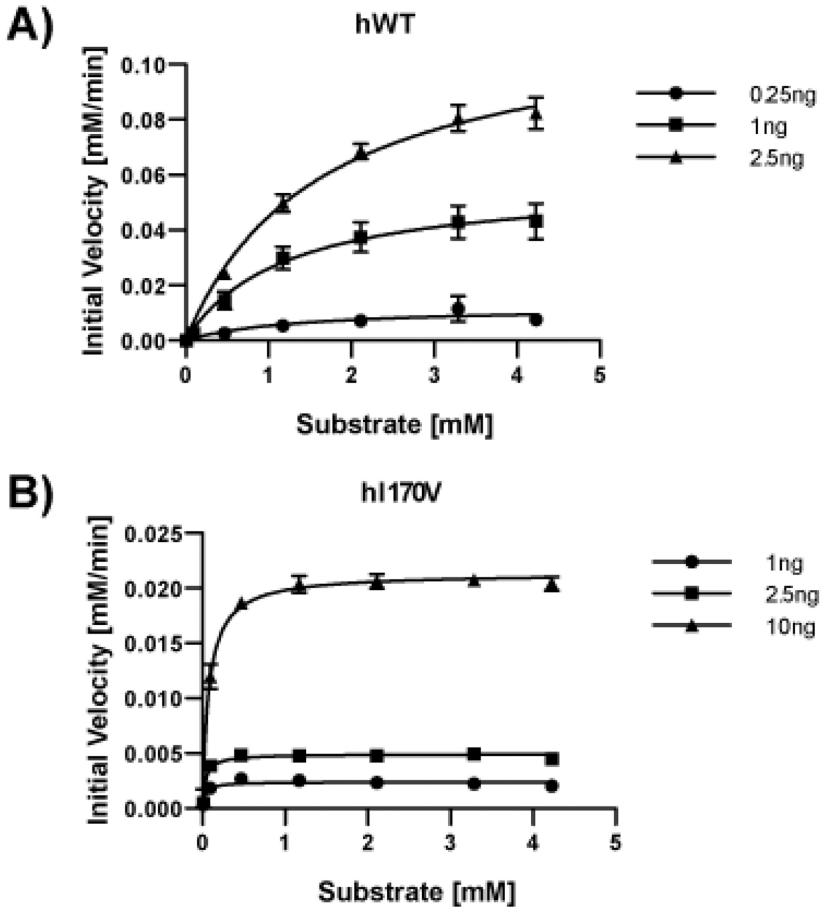

C)

	hTPI^{WT}	hTPI^{I170V}
K_m (GAP) (mM)	1.4 ± 0.1	0.049 ± 0.014
k_{cat} (GAP) (s^{-1})	1623 ± 181.1	75.8 ± 2.6
k_{cat}/K_m (GAP) (M^{-1} s^{-1})	1.2 x 10^6	1.5 x 10^6

Fig. 3.

hTPI^{I170V} reduces K_m and catalytic turnover. hTPI^{WT} and hTPI^{I170V} display typical Michaelis Menten kinetic profiles (A,B). I170V reduces K_m and catalytic turnover (C). Error bars and ± indicate S.E.M.

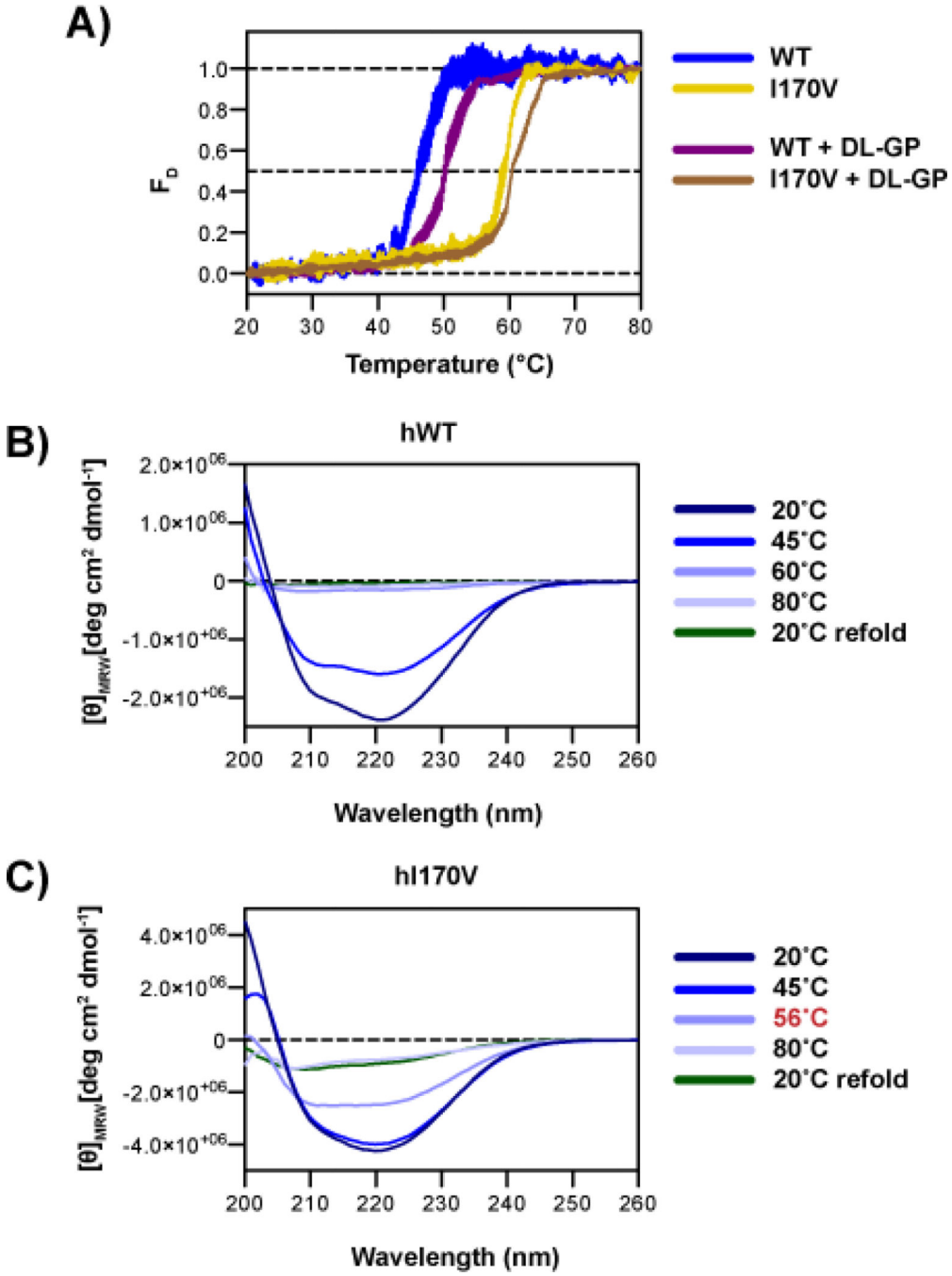

Fig. 4.

I170V enhances TPI stability relative to WT. CD thermal shift analyses demonstrate a stabilization of TPI due to the I170V substitution (A), and responsiveness to catalytic site occupancy via DL-GP substrate analog (A). Far-UV spectra demonstrate similar folding between $hTPI^{WT}$ (B) and $hTPI^{I170V}$ (C), with averaged spectra from selected temperatures (B,C). No refolding was noted in either enzyme. Error bars represent S.D.

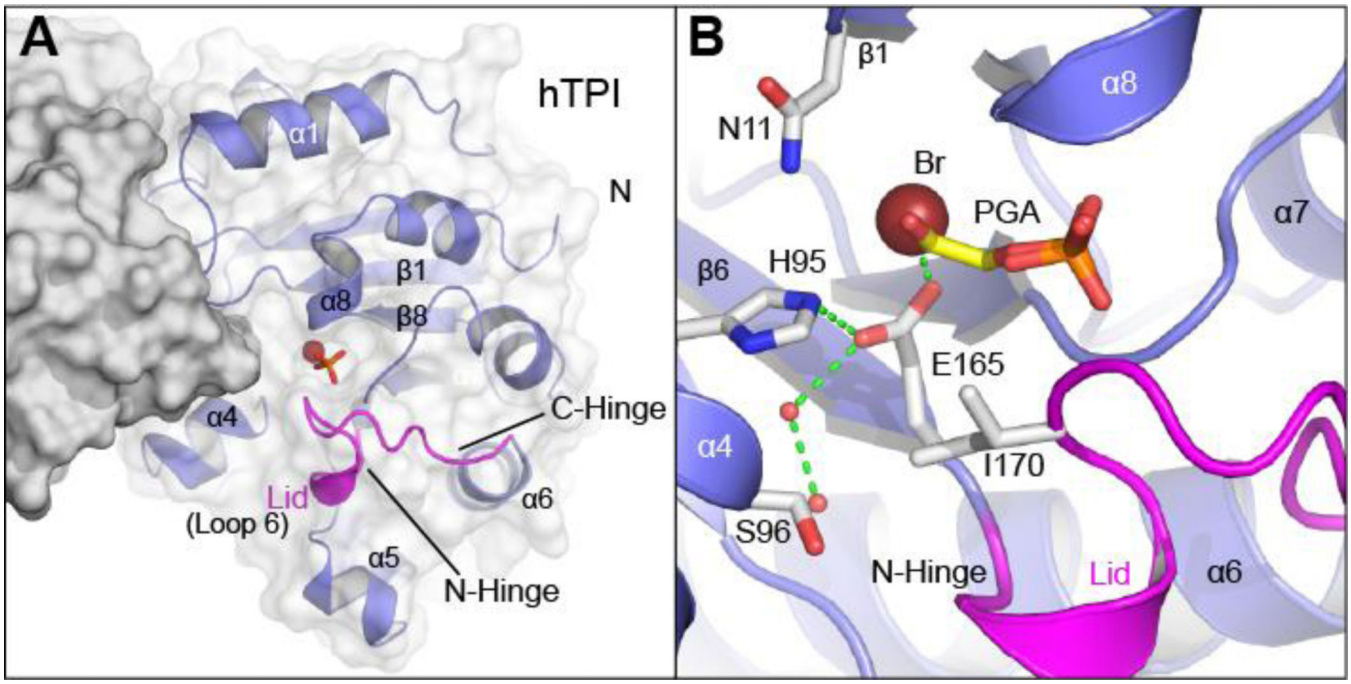

Fig. 5.

Architecture of WT and hTPI^{I170V}. (A) Overview of wild-type hTPI dimer with one subunit indicated as a solid grey surface while the other is represented in both cartoon (blue) and semitransparent surface (white). The position of the loop 6, which forms the lid and completes the active site pocket is indicated in magenta. The canonical nomenclature for landmark secondary structure elements is indicated. (B) The positions of bromide and phosphate ions observed in hTPI^{WT} is indicated. The position of the substrate analog PGA within the catalytic pocket as positioned via structural alignment of TPI is indicated (PDB: 1HTI) [48]. Only the PGA from this alignment is shown for clarity. The network of hydrogen bonding connecting critical catalytic residues are indicated by green dashes.

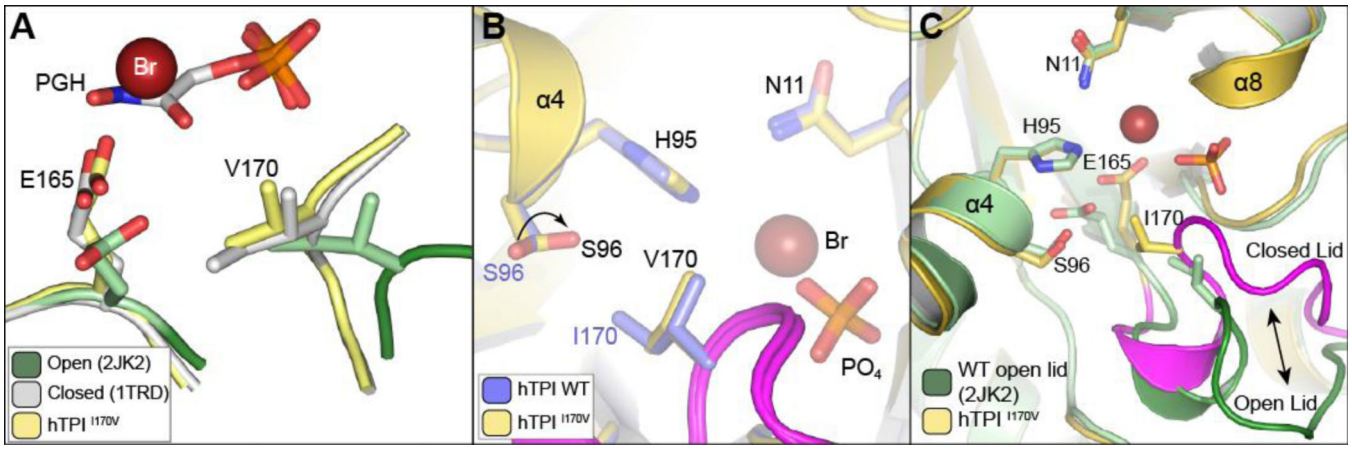

Fig. 6.

The I170V substitution decouples S96 positioning from lid closure. (A) Substitution of valine at position 170 does not alter E165 or loop 6 positioning within the closed lid state. The structures of hTPI^{I170V} (yellow), PGH-liganded TPI (PDB 1TRD, grey), and TPI in an unliganded open state (PDB 2JK2, green) were superposed and the positions of E165 and I170 are indicated (B). Repositioning of S96 within a closed lid structure in I170V. View of the catalytic pocket after structural alignment of WT (Blue) and I170V (Gold) hTPI structures. The catalytically important residues S96, H95, and N11 are shown as sticks. The catalytic residue E165 is unchanged and is omitted for clarity. The lid for both structures are indicated in magenta. (C) hTPI^{I170V} adopts a closed lid conformation. The active site from a structural alignment of hTPI^{WT} (green) in an open lid conformation (2JK2) [4] and hTPI^{I170V} (gold) is shown. The positions of the lids and respective active site residues are indicated.

Table 1

Data collection and refinement statistics

Data Collection	**TPI^{WT}**	**TPI^{I170V}**
Space Group	$P2_1$	$P2_12_12_1$
Cell Dimensions		
a (Å)	47.92	63.65
b (Å)	48.85	70.73
c (Å)	93.97	91.74
β (°)	103.66	
Resolution (Å)	50-1.60 (1.63–1.60)	40.0-2.00 (2.03–2.00)
Unique Reflections	52,340	27,738
R_{merge}	7.7 (44.2)	13.9 (47.4)
$I/\sigma I$	40.9 (2.0)	16.2 (2.0)
Completeness (%)	93.8 (54.2)	95.5 (67.4)
Redundancy	5.6 (3.0)	4.8 (1.7)
Refinement		
Resolution (Å)	46.60-1.60	38.94-2.00
R_{work} / R_{free} (%)	15.30 / 18.73	17.04 / 21.31
Number of atoms	4058	3972
Protein	3722	3695
Water	326	268
Other	10	9
R.m.s. deviations		
Bond lengths (Å)	0.005	0.004
Bond angles (°)	0.962	0.779
Average isotropic B values (Å^2)	36.13	35.24
Protein	35.73	35.07
Solvent	40.68	37.55
Ramachandran (%)		
Favored	97.34	97.12
Allowed	2.66	2.88
Outliers	0.00	0.00

Values in parentheses correspond to those in the outer resolution shell.

R_{merge} = (|(ΣI - <I>)|)/(ΣI), where <I> is the average intensity of multiple measurements.

$R_{work} = \Sigma_{hkl}||F_{obs}(hkl)|| - F_{calc}(hkl)||/\Sigma_{hkl}|F_{obs}(hkl)|$.

R_{free} = crossvalidation R factor for 5% of the reflections against which the model was not refined.